Annals of Biomedical Engineering, Vol. 21, pp. 679-697, 1993
Printed in the USA.

0090-6964/93 $6.00 + .00

Quantitative Characterization of Cell Invasion *In Vitro*: Formulation and Validation of a Mathematical Model of the Collagen Gel Invasion Assay

RICHARD B. DICKINSON,* JAMES B. MCCARTHY,† and ROBERT T. TRANQUILLO*

Departments of *Chemical Engineering and Materials Science and
†Laboratory Medicine and Pathology, University of Minnesota, Minneapolis, MN

Abstract—An *in vitro* assay proposed to systematically characterize and compare cell invasion under different conditions is the collagen gel invasion assay where cells, initially seeded onto the surface of a type I collagen gel, penetrate the surface and migrate within the gel over time. Using simplifying assumptions about cell transport across the gel surface and migration within the gel, we formulate and solve a mathematical model of this assay which predicts the resulting cell distribution based on three phenomenological parameters characterizing the ability of cells to penetrate the gel surface interface, migrate randomly within the gel, and return to the gel surface. An index of cell invasiveness is defined based on these parameters that reflects the overall ability of cells to transport across the gel surface interface, that is, invade the gel. Cell concentration profiles predicted by the model correspond well to measured profiles for murine melanoma cells invading gels supplemented with extracellular matrix proteins fibronectin and type IV collagen as well as unsupplemented gels, allowing these parameters to be estimated by a nonlinear regression fit of the model solution to the measured profiles. Our analysis suggests that type IV collagen and fibronectin primarily modulate cell transport across the gel surface interface rather than migration within the gel. Further, we validate the key model assumptions and obtain independent, direct estimates of model parameters by time-lapse video microscopy and digital image analysis of cell penetration of the gel surface and migration within the gel during the assay.

Keywords—Invasion, Collagen gel, Mathematical model, Metastasis, Migration, Cell tracking.

INTRODUCTION

The ability of blood and tissue cells to penetrate into and migrate through extracellular matrix is essential to physiological processes such as inflammation, wound healing, embryogenesis, and tumor cell metastasis. In the inflammatory response, neutrophils extravasate by penetrating vascular basement membrane then migrating through connective tissue to the site of infection (30). In the process of wound repair, neutrophils, monocytes, endothelial cells and fibroblasts must infiltrate the fibrin matrix of the blood clot (20). In embryonic heart development, mesenchymal cells penetrate and then migrate through an extracellular matrix barrier toward the myocardium (24). A notorious example is tumor cell invasion in the process of metastasis. In several steps of this process, tumor cells actively penetrate basement membrane and then migrate through connective tissue before finally arresting and proliferating at the secondary tumor site (18).

Several *in vitro* assays have been developed to investigate the invasive behavior of blood and tissue cells. These include human amnion (25), reconstituted basement membrane (7), reconstituted fibrin gels (13,21), and reconstituted collagen gels (28) as model tissues. Although these assays differ in their advantages and disadvantages as models of cell invasion *in vivo*, they are similar in methodology: Cells are seeded onto the surface of the model tissue, and over time, penetrate the surface then migrate within the tissue, even migrating across the relatively thin tissues used in some invasion assays. The resulting distribution of the cell population is quantified. In this work, we focus on the collagen gel invasion assay, although many of the methods and results presented here can be extended to similar assays.

A schematic of the collagen gel invasion assay is presented in Fig. 1. Initially, cells are uniformly dispersed on the surface of the gel, and then during incubation, penetrate the surface and migrate within the gel. Convenient measurements are the total number of cells invaded per unit area and the number of cells which have migrated to various depth levels, termed the cell concentration profile. Typical results from this assay are presented in Fig. 2 for cells from a highly metastatic cell line (clone M4 of the K1735 murine amelanotic melanoma cell line, hereafter referred to as M4 cells) where the concentration profiles of cells invading a gel supplemented with type IV collagen or with fibronectin are compared to that of cells

Acknowledgments—This work has been supported by a National Science Foundation PYI Award (BCS-8957736) and matching funds from the Procter & Gamble Company to RTT.

Address correspondence to Robert T. Tranquillo, Dept. of Chemical Engineering and Materials Science, University of Minnesota, Minneapolis, MN 55455.

(*Received 3/25/93*)

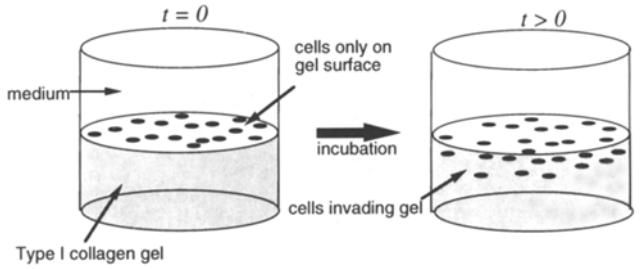

FIGURE 1. Schematic of the collagen gel invasion assay. At $t = 0$, cells are seeded uniformly on the gel surface. Over time, cells invade by penetrating the gel surface and migrating within the gel.

invading an unsupplemented gel (see Appendix for Materials and Methods). These data suggest that the supplements affect the number of cells at each depth level, although the "leading front distance" (the depth of the gel at which the cell number becomes very small) is approximately the same in each case.

Interpreting such results for different gel compositions in relation to cell invasiveness raises a critical question: Does the difference between the cell concentration profiles arise from differences in cell penetration of the gel surface, or from differences in cell migration within the gel? Either possibility or a combination of both is plausible without further analysis. This question is further complicated by the possibility of different cell division rates. We propose a mathematical model of the collagen gel invasion assay to resolve this question and facilitate interpretation of such experimental results. This is possible with the model's objective index of cell invasiveness, which can be estimated by fitting the solution to the model equations to the measured cell concentration profiles. The model formulation involves simplifying assumptions about cell penetration of the gel surface, migration within the gel, and return to the gel surface. The model utilizes three phenomenological parameters that characterize cell penetration, migration, and the equilibrium partitioning of cells between the gel interior and the gel surface. From these parameters, we postulate an objective index of invasiveness which reflects the overall ability of the cells to transport across the surface into the gel (involving penetration, migration, and return), that is, to invade the gel. The model predictions of cell concentration profiles are compared qualitatively to the experimental data presented in Fig. 2 to elucidate the controlling phenomena, and quantitatively via nonlinear regression to estimate the model parameters.

To further determine the validity of the model assumptions and obtain *independent* estimates of the model parameters, we employ an automated optical microscope/image processing workstation to directly observe cell behavior during the assay by simultaneous time-lapse video microscopy of multiple fields of the gel surface. From these time-lapse sequences, we measure the residence times of cells on the gel surface and track cells migrating within the gel using a novel methodology. From the resulting data, we obtain direct estimates of the corresponding model parameters and find good agreement between these values and those estimated by fitting the model solution to the cell concentration profiles measured in the assay.

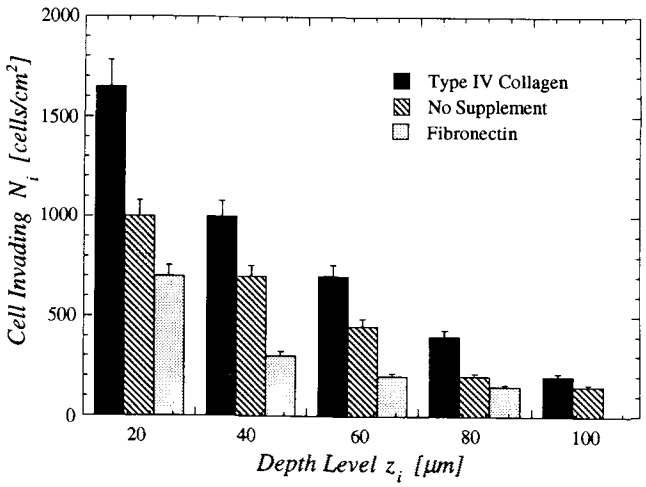

FIGURE 2. Representative cell concentration profiles measured in the collagen gel invasion assay. The bars represent the number of M4 cells/cm^2 in various 20 μm increments of the gel depth after 3 days of incubation. Error bars represent the theoretical statistical uncertainty in estimating mean values by counting a finite number of cells.

MATHEMATICAL MODEL FORMULATION AND ANALYSIS

Our approach is to make the most simplifying assumptions which suitably represent cell behavior within the assay, as justified by validation of the model predictions (see "Validation" section). As shown schematically in Fig. 3, we assume that cells penetrate the surface of the gel and return to the surface when immediately beneath it with probabilities per unit time, k_+ and k_-, respectively, which are independent of position on the gel surface and constant over the duration of the experiment (k_+ and k_- are equivalent to interfacial transport rate constants, as will be evident in the governing equations, implying the existence of a gel surface interface). The ratio, $K = k_-/k_+$, defines an equilibrium partition coefficient for the cells on the gel surface to cells within the gel.

We also assume that cells within the gel exhibit random migration with mean speed and turning probability which are independent of position and constant over the duration of the experiment. The theory for modeling random migration derives from an underlying probabilistic

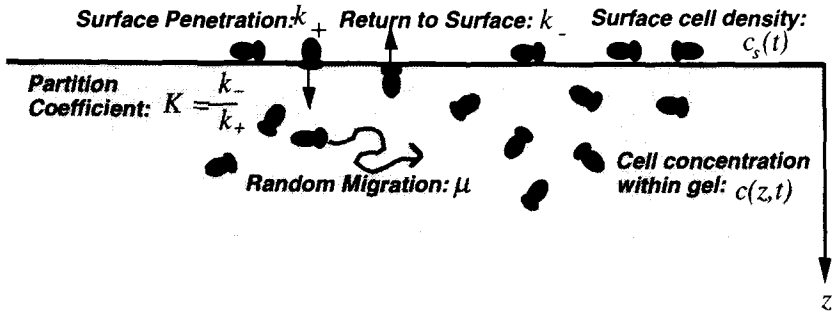

FIGURE 3. Schematic showing the model assumptions. Cell penetration of the gel surface and return to the surface are characterized by the interfacial transport rate constants k_+ and k_-, respectively. Random cell migration within the gel is characterized by the random motility coefficient, μ. $K = k_-/k_+$, is the equilibrium partition coefficient.

model of cell movement and describes the expected migration of a cell population, reflecting a large number of individual cell paths (6,23). There is a complete analogy between Fick's Law

$$J_n = -D\frac{\partial c_n}{\partial z} \tag{1}$$

describing the molecular flux, J_n, associated with diffusion down a molecular concentration gradient, $\partial c_n/\partial z$, (the manifestation of Brownian motion due to molecular collisions) and the theoretical result describing the flux of cells, J, associated with random motility down a cell concentration gradient, $\partial c/\partial z$, (the manifestation of cell random turning behavior in an isotropic environment)

$$J = -\mu\frac{\partial c}{\partial z} \tag{2}$$

Also analogous are the molecular diffusion coefficient, D, appearing in Fick's law and the random motility coefficient, μ, appearing in the cell migration theory, with μ reflecting both the cell speed and the frequency of directional changes. Here we implicitly assume that the cell population under observation is sufficiently large such that a continuum definition of cell concentration in the gel, c [cells/volume], is valid (this can be experimentally imposed). Likewise, we define c_s [cells/area] as the two-dimensional cell concentration on the gel surface. Finally, we account for the possibility that cell division may occur on the surface and within the gel, with associated first-order rate constants, k_{gs} and k_g, respectively. The cell population is assumed to be largely homogeneous with respect to the above properties.

The assumption that the parameters k_+, k_-, μ, k_{gs}, and k_g are independent of position and constant over the duration of the experiment implies that "mediator effects" associated with the time-dependent accumulation of cell-derived factors or depletion of nutrients that influence the cell behavior or gel properties are negligible. The assumptions also imply that the cell population is disperse enough such that the effects of cell-cell contacts are negligible. In general, these conditions can be experimentally imposed using a relatively low initial surface cell concentration.

With these assumptions, we formulate cell conservation equations for the gel surface and interior which govern the time evolution of $c_s(t)$ and $c(z,t)$ at any time, t, and depth, z:

$$\frac{dc_s(t)}{dt} = -k_+c_s(t) + k_-c(0,t) + k_{gs}c_s(t) \tag{3}$$

$$\frac{\partial c}{\partial t} = -\frac{\partial J}{\partial z} + k_gc(z,t) \tag{4}$$

where J in Eq. 4 is defined by Eq. 2. One boundary condition is obtained by matching the cell fluxes at the gel surface, $z = 0$, such that

$$-\mu\frac{\partial c(0,t)}{\partial z} = k_+c_s(t) - k_-c(0,t) \tag{5}$$

A second results from stipulating that the bottom of the assay chamber is too deep to be reached by cells during the incubation period, and therefore is essentially at $z = \infty$ (experimentally imposed). Thus, the cell concentration approaches zero far from the gel surface, i.e.

$$c(z \to \infty, t) = 0 \tag{6}$$

The initial condition is simply that all cells are present on the gel surface at concentration c_{s0}, so

$$c_s(0) = c_{s0} \tag{7}$$

$$c(z,0) = 0 \tag{8}$$

The result of this formulation is a coupled pair of linear differential equations which are solved analytically by the method of Laplace transforms to obtain explicit expressions for $c_s(t)$ and $c(z,t)$. For the case where the specific growth rate within the gel is equal to that on the surface, i.e. $k_g = k_{gs}$, the solution is

$$c_s(t) = \frac{c_{s0}}{2}\exp(k_g t)\left\{\left(\frac{1}{\beta}+1\right)\exp(\nu^2)\operatorname{erfc}(\nu) - \left(\frac{1}{\beta}-1\right)\exp(\rho^2)\operatorname{erfc}(\rho)\right\} \quad (9)$$

$$c(z,t) = \frac{c_{s0}}{K}\exp(k_g t - \delta^2) \times \frac{1}{\beta}\left(\exp[(\delta+\nu)^2]\operatorname{erfc}[\delta+\nu] - \exp[(\delta+\rho)^2]\operatorname{erfc}[\delta+\rho]\right) \quad (10)$$

involving the following dimensionless groups and variables:

$$\beta = \left(1 - \frac{4}{\phi^2}\right)^{1/2} \quad (11)$$

$$\delta = \frac{z}{(4\mu t)^{1/2}} \quad (12)$$

$$\nu = \tfrac{1}{2}\phi(1-\beta)(k_+ t)^{1/2} \quad (13)$$

$$\rho = \tfrac{1}{2}\phi(1+\beta)(k_+ t)^{1/2} \quad (14)$$

$$\phi = \left(\frac{k_+ K^2}{\mu}\right)^{1/2} \quad (15)$$

When β is imaginary, Eqs. 9 and 10 can be written as

$$c_s(t) = c_{s0}\exp(k_g t)\frac{1}{|\beta|}\operatorname{Im}(w(\zeta)) + \operatorname{Re}(w(\zeta)) \quad (16)$$

and

$$c(z,t) = \frac{c_{s0}}{K}\exp[-(\delta^2 + k_g t)]\frac{2}{|\beta|}\operatorname{Im}[w(2\delta i + \zeta)] \quad (17)$$

where

$$\zeta = \tfrac{1}{2}\phi(k_+ t)^{1/2}(|\beta| + i) \quad (18)$$

and $w(\zeta)$ is a tabulated complex function (1) defined for (possibly complex) ζ by

$$w(\zeta) = \exp(-\zeta^2)\operatorname{erfc}(-i\zeta) \quad (19)$$

In the more general case, where $k_g \neq k_{gs}$, the solution is

$$\frac{c_s(t)}{c_{s0}} = \frac{Ae^{k_g t}}{(a^2 - k_{gs}/k_+ + k_g/k_+ + 1)}w(-ia(k_+ t)^{1/2}) + \frac{Be^{k_g t}}{(b^2 - k_{gs}/k_+ + k_g/k_+ + 1)}w(-ib(k_+ t)^{1/2}) + \frac{Ce^{k_g t}}{(c^2 - k_{gs}/k_+ + k_g/k_+ + 1)}w(-ic(k_+ t)^{1/2}) \quad (20)$$

$$\frac{c(z,t)K}{c_{s0}} = e^{k_g t - \delta^2}\{Aw[i(\delta - a(k_+ t)^{1/2})] + Bw[i(\delta - b(k_+ t)^{1/2})] + Cw[i(\delta - c(k_+ t)^{1/2})]\} \quad (21)$$

where

$$A = \frac{a\phi}{(a-b)(a-c)} \quad (22)$$

$$B = \frac{b\phi}{(b-a)(b-c)} \quad (23)$$

$$C = \frac{c\phi}{(c-a)(c-b)} \quad (24)$$

and a, b, and c are the three roots to the cubic equation

$$x^3 + \phi x^2 + \left(1 - \frac{k_{gs} - k_g}{k_+}\right)x + \phi\frac{k_{gs} - k_g}{k_+} = 0 \quad (25)$$

(If two roots of Eq. 25 are complex conjugates, the imaginary components of Eqs. 20 and 21 cancel.)

Model predictions for $c_s(t)$ and $c(z,t)$ are plotted in Fig. 4 for hypothetical values of the model parameters. As shown in Fig. 4b, the prediction of the cell concentration profile, $c(z,t)$, in the absence of cell division is qualitatively similar to that for the classical problem of diffusive transport into a semi-infinite medium (4) (which assumes no depletion of the diffusing component at the interface and no resistance to transport across the interface); however, the effect of depletion of cells on the gel

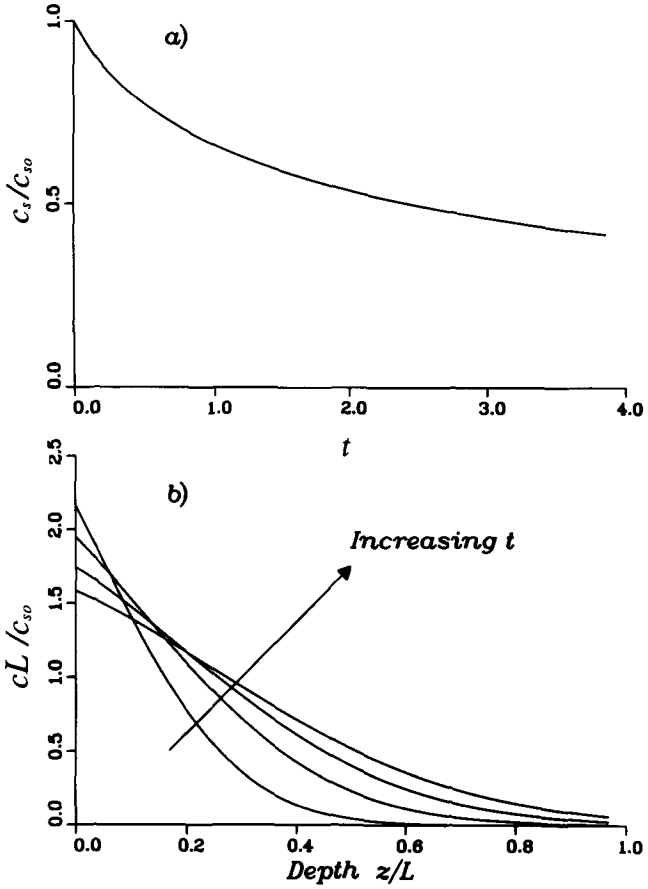

FIGURE 4. Representative model predictions of the dimensionless (a) surface cell concentration, $c_s(t)/c_{s0}$, vs. time, t, and (b) cell concentration, $c(z,t)L/c_{s0}$, vs. dimensionless depth, z/L, for L = 200 μm, t = 1,2,3,4 days, $k_+ = 0.3$ day^{-1}, $K = 40$ μm, and μ = 1000 μm^2/day ($k_{gs} = k_g = 0$).

surface is evident in the cell concentration profile, i.e. $c(z,t)$ *decreases* in time for z close to 0.

In general, the model solution depends on three phenomenological parameters k_+, μ, and K (hereafter, k_g and k_{gs} are assumed to have known values and, hence, are not considered "parameters" in our analysis). The penetration rate constant, k_+, reflects the ability of cells to penetrate the gel surface. The random motility coefficient, μ, reflects the ability of cells to migrate randomly in the gel. The partition coefficient, K, reflects the concentrations of cells on the gel surface relative to the gel interior that would exist at equilibrium. The sensitivity of the solution to these parameters is shown in Fig. 5. Note that the dependencies of the cell concentration profile, $c(z,t)$, on the parameters k_+ and K are qualitatively similar. Varying k_+ or K significantly changes the cell concentration at most depths but not the depth at which the cell concentration becomes very small (i.e. the "leading front distance"). Varying μ, on the other hand, greatly affects the leading front distance. This difference will be exploited below when applying the model to the experimental data.

The square of the dimensionless parameter, ϕ, defined by Eq. 15, is an important combination of these parameters and reflects the ratio of the time scale of cell transport from the gel surface interface via migration before cells return to the surface (characterized by the ratio K^2/μ) to the time scale of cell penetration of the surface (characterized by $1/k_+$). Depending on the value of ϕ^2 and the time scale of the assay, the general solution for $c_s(t)$ and $c(z,t)$ which depends on three parameters reduces to several interesting limits that depend on at most two parameters (for simplicity, we present here only the limits of Eqs. 9 and 10 for the case $k_g = k_{gs}$). If $\phi^2 \gg 1$, cell transport into the gel is "migration-limited" and independent of k_+ explicitly, depending only on K and μ. The limiting solution in this case for an intermediate time scale, $t = O(K^2/\mu)$, is

$$c_s(t) = c_{s0}e^{k_g t}\exp\left(\frac{\mu t}{K^2}\right)\mathrm{erfc}\left(\left(\frac{\mu t}{K^2}\right)^{1/2}\right) \tag{26}$$

$$c(z,t) = \frac{c_{s0}}{K}e^{k_g t}\exp\left(\frac{\mu t}{K^2} + \frac{z}{K}\right)\mathrm{erfc}\left(\left(\frac{\mu t}{K^2}\right)^{1/2} + \delta\right) \tag{27}$$

This limit is seen in Figs. 5a,b, where for very large k_+, $c_s(t)$ and $c(z,t)$ become independent of k_+ and the profiles superimpose. In addition, on a short time scale such that $t \ll K^2/\mu$, during which there is negligible depletion of cells from the gel surface, Eqs. 26 and 27 simplify further to become

$$c_s = c_{s0}e^{k_g t} \tag{28}$$

$$c(z,t) = \frac{c_{s0}}{K}e^{k_g t}\mathrm{erfc}(\delta) \tag{29}$$

which in the absence of cell division ($k_g = 0$) is mathematically equivalent to the solution for the classical problem of "free diffusion" into a semi-infinite medium (4).

Conversely, if $\phi^2 \ll 1$, cell transport into the gel is "penetration-limited", whereby the solution becomes independent of the partition coefficient, K, and dependent only on k_+ and μ. The limiting solution for this case is

$$c_s(t) = c_{s0}\exp[(k_g - k_+)t] \tag{30}$$

$$c(z,t) = c_{s0}e^{k_g t}(k_+/\mu)^{1/2}\exp(-\delta^2) \times \mathrm{Im}\{w[(k_+ t)^{1/2} + i\delta]\} \tag{31}$$

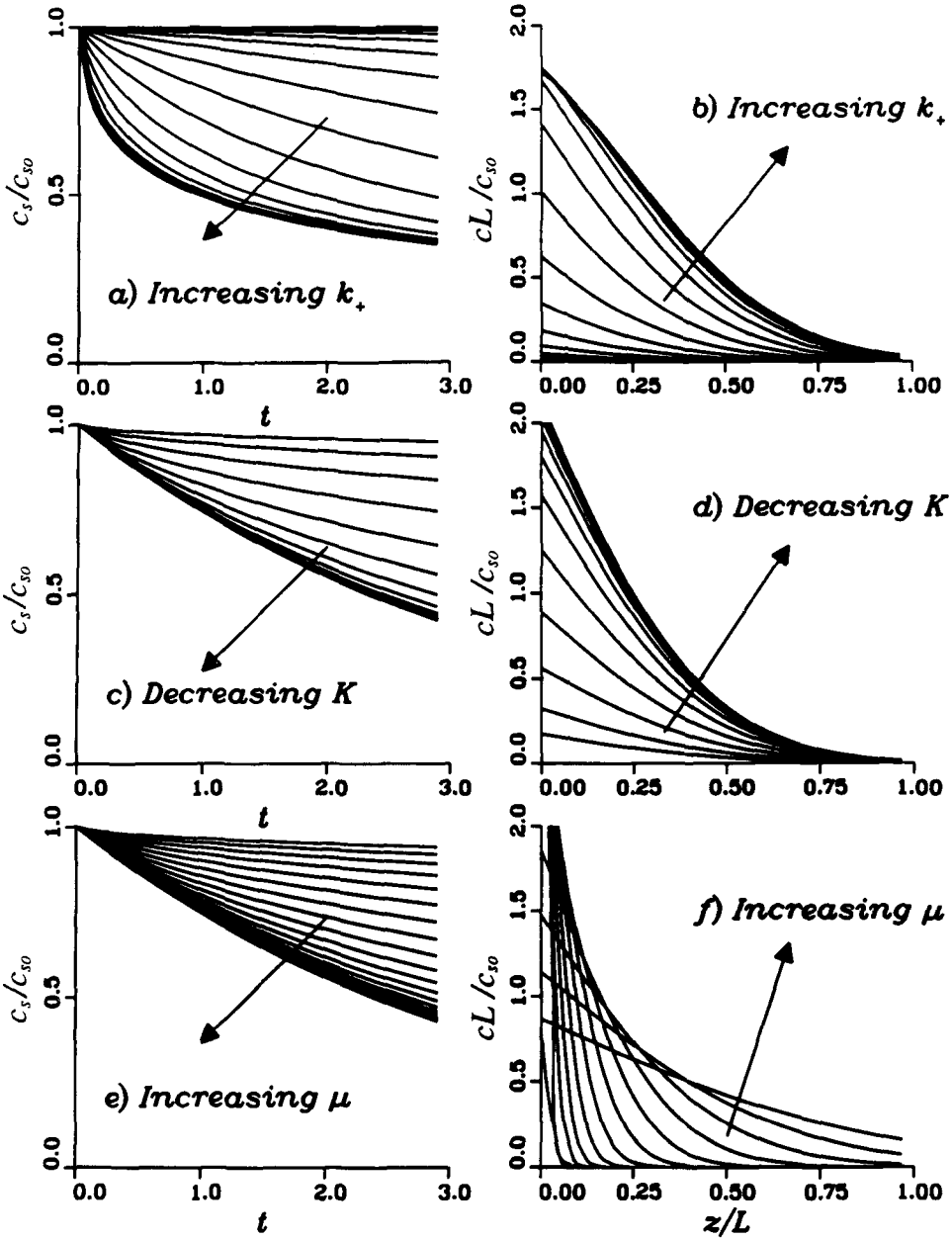

FIGURE 5. Model predictions of the (a,c,e) surface cell concentration, $c_s(t)/c_{so}$, and (b,d,f) cell concentration profiles, $c(z,t)L/c_{so}$, at $t = 3$ days are shown for varying parameters μ (a,b), k_+ (c,d), and K (e,f), where in each case all unvaried parameters have the same values as in Fig. 4.

This limit is evident in Figs. 5c–f. As K becomes very small or μ becomes very large (so that $\phi^2 \ll 1$), $c_s(t)$ becomes independent of these two parameters, consistent with Eq. 30.

Regardless of the value of ϕ^2, on a long time scale relative to the time scale of cell transport, i.e. $t \gg 1/k_+$ and $t \gg K^2/\mu$, Eqs. 9 and 10 become

$$c_s(t) = 0 \tag{32}$$

$$c(z,t) = \frac{c_{so}}{(\pi\mu t)^{1/2}} \exp(k_g t - \delta^2) \tag{33}$$

On this time scale, the gel surface interface effectively presents no resistance to cell transport such that all cells are located just beneath the interface (within the gel) initially. This is consistent with the cell concentration profiles being independent of k_+ and K as seen in Eq. 33. Note that in the absence of cell division ($k_g = 0$), Eq. 33 is

mathematically equivalent to the solution to the classical problem of diffusion away from a plane source in an infinite medium (4).

We now wish to define an objective index that reflects overall cell invasiveness and can be estimated by fitting the model solution to experimental cell concentration profiles. The implication of the above limits is that for some regions of parameter space, it is impossible to obtain independent estimates of all three phenomenological parameters of interest, k_+, K, and μ. It is also clear that to successfully invade the gel, i.e. transport across the gel surface interface, a cell must penetrate the gel surface *and* migrate away before returning to the surface. This is analogous to two interfacial resistances in series. The proposed invasiveness index, η, should thus be a function of objective parameters that can be estimated and reflect the overall ability of the cell to overcome both "resistances." Furthermore, η should be defined for both "migration-limited" ($\phi^2 \gg 1$) and "penetration-limited" ($\phi^2 \ll 1$) regions of parameter space. A definition for η which fits these criteria based on the generic series resistance formula is

$$\eta = \frac{1}{\frac{1}{k_+} + \frac{K^2}{\mu}} \tag{34}$$

or equivalently

$$\eta = \frac{k_+}{1 + \phi^2} = \frac{\mu/K^2}{\frac{1}{\phi^2} + 1} \tag{35}$$

From Eq. 35, we see that for $\phi^2 \ll 1$, $\eta = k_+$, consistent with the "penetration-limited" limit to cell invasion, and for $\phi^2 \gg 1$, $\eta = \mu/K^2$, consistent with the "migration-limited" limit to cell invasion.

APPLICATION OF THE MODEL TO EXPERIMENTAL CELL CONCENTRATION PROFILES AND ESTIMATION OF PARAMETER VALUES

The utility of the mathematical model is first demonstrated by comparing model predictions to the experimental data presented in Fig. 2. Since the gel supplements do not significantly affect k_{gs} for M4 cells on a type I collagen gel and $k_g = k_{gs}$ can be assumed (see Appendix), a qualitative comparison between the experimental cell concentration profiles presented in Fig. 2 and the model predictions parameterized on k_+, K, and μ presented in Fig. 5 is legitimate. This comparison suggests that since the supplements affect the number of cells at each depth level rather than the leading front distance, they therefore affect either the penetration rate constant, k_+, and/or the partition coefficient, K, rather than the random motility coefficient, μ. This suggests that the supplements modulate cell behavior at the gel surface rather than behavior within the gel. As shown in Figs. 6 and 7, this conclusion is supported by a nonlinear least squares regression fit of the model solution to the experimental profiles to estimate model parameters (the analysis indicates that, in all three cases, cell invasion is "migration-limited" allowing only μ and K to be reliably estimated, so only μ and $\eta = \mu/K^2$ are reported in Fig. 7). The regression estimates of η significantly differ for the supplemented gels relative to the unsupplemented control. However, the estimates of μ are nearly the same in each case. The model predictions, therefore, support the conclusion that the supplements modulate transport across the gel surface interface, but not the random migration of cells within the gel. Specifically, the type IV collagen supplement enhances invasiveness, whereas the fibronectin supplement inhibits invasiveness. Furthermore, the model provides *objective*, quantitative measures of gel invasiveness (η) and random migration within the gel (μ).

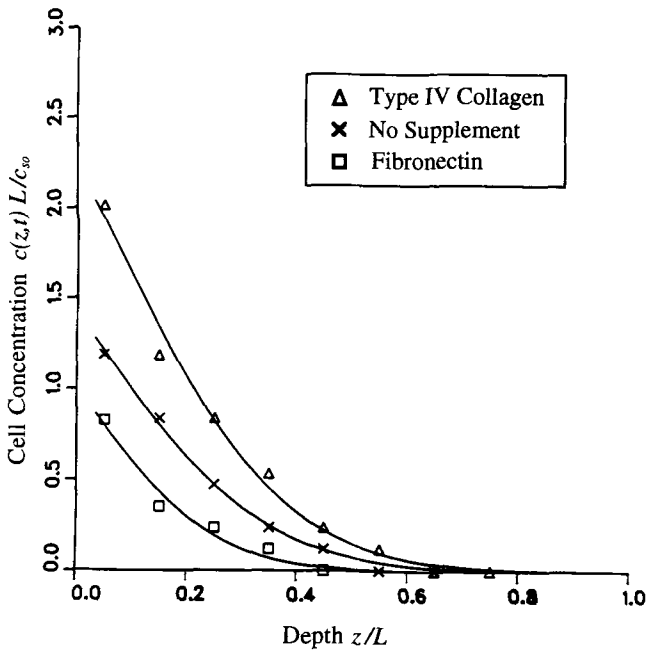

FIGURE 6. Nonlinear least squares regression fits (lines) of the model solution, Eqs. 9 and 10, to the experimental data (points) presented in Fig. 2 for parameter estimation (t = 3 days, L = 200 μm, and $k_g = k_{gs} = 0.23$ day^{-1} is assumed—see Appendix).

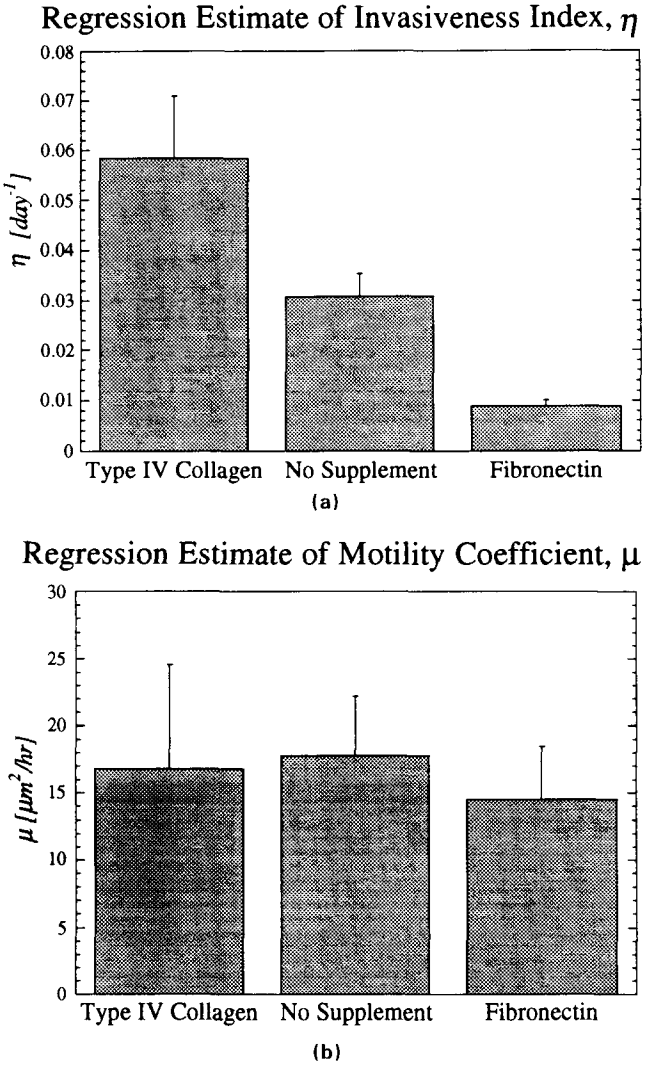

FIGURE 7. Estimates of (a) invasiveness index, η, and (b) random motility coefficient, μ, obtained from the nonlinear least squares regression fits in Fig. 6. The analysis provided parameter estimates yielding large ϕ^2 ($\approx$40) and large standard error in the estimate of k_+ indicating "migration-limited" cell invasion. The data were then refitted using the limiting solution, Eqs. 26 and 27, to estimate μ and K, allowing calculation of $\eta = \mu/K^2$. Error bars indicate standard errors in the parameter estimates from the regression analysis.

VALIDATION OF MODEL ASSUMPTIONS AND DIRECT ESTIMATION OF PARAMETER VALUES

Based on Fig. 6, there appears to be excellent agreement between the model predictions of cell concentration profiles and the data for M4 cells invading the three gel types. The predicted cell concentration profiles also show good qualitative agreement with published data for other cell types invading type I collagen gels, for example, neutrophils (3,13,15), lymphocytes (27), and adenocarcinoma cells (22). This agreement suggests that the assumptions underlying the model equations are at least accurate enough to provide reasonable predictions of cell concentration profiles for a variety of cell types. To further validate the key model assumptions and accuracy of its parameter estimates, we directly observed M4 cell behavior in the collagen gel invasion assay, both cell penetration of the gel surface and cell migration within the gel.

Using methods described in the Appendix, cells within the collagen gels were tracked to (a) validate the assumption that cells move by random migration such that Eq. 2 applies, and (b) obtain a *direct* estimate of the random motility coefficient, μ, for each gel type for comparison to values estimated from fitting the model solution to the experimental data (Figs. 6 and 7b). It has been theorized and documented that the random migration of an individual cell can be adequately modeled as a persistent random walk, whereby the time correlation in the movement direction is finite and characterized by a parameter termed the "directional persistence time", P (6,23). The mean-squared displacement of the cell, $\langle d^2(t)\rangle$, over any time increment, t, is then given by the relation

$$\langle d^2(t)\rangle = 2n\mu(t - P(1 - \exp(-t/P))) \qquad (36)$$

where n is the dimensionality in which $\langle d^2\rangle$ is measured (For example, if cell movement in three dimensions, x, y, and z, is measured, then $\langle d^2\rangle = \langle d_x^2 + d_y^2 + d_z^2\rangle$ and $n = 3$. However, if only the *projected* cell tracks are analyzed such that $\langle d^2\rangle$ is measured as $\langle d_x^2 + d_y^2\rangle$, then $n = 2$). For $t \gg P$, Eq. 36 reduces to

$$\langle d^2(t)\rangle = 2n\mu t \qquad (37)$$

so that $\langle d^2(t)\rangle$ is proportional to t, characteristic of a spatial diffusion process. This implies that if Eq. 36 is experimentally confirmed and the duration of the assay is long relative to P, then use of the constitutive cell flux equation defined in Eq. 2 is valid.

For unsupplemented gels of type I collagen, and gels supplemented with type IV collagen and fibronectin, individual cells within the gels were imaged via time-lapse video microscopy, cell tracks were constructed via a cell matching algorithm, and $\langle d^2(t)\rangle$ was computed from the constructed cell tracks, which are projections into the focal plane of the gel surface, as presented in Fig. 8 (see Appendix for methods). μ and P were determined by fitting Eq. 36 to the data with nonlinear least squares regression. In each case, P was found to be negligible (i.e., $P < 20$ min), most likely due to the tortuous fibrillar structure of the collagen gel. In Fig. 9, the values of μ so estimated by cell tracking are compared to those estimated from the fits of the model solution to the experimental cell concentration profiles. Although the directly estimated values of μ are slightly higher than those estimated via the model, the agreement is quite close and the same

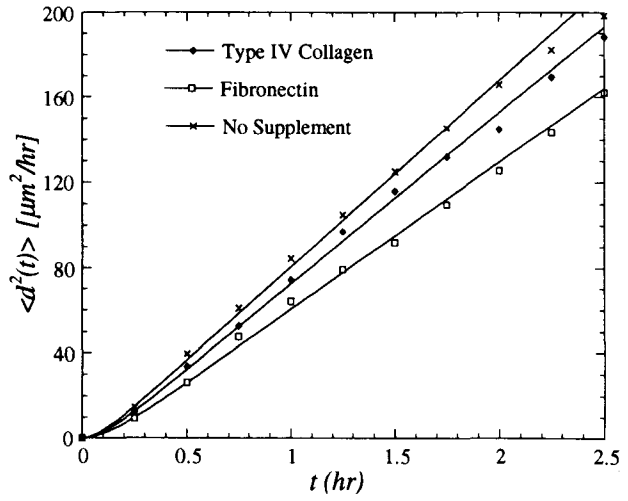

FIGURE 8. Plot of mean-squared displacement vs. time, t, based on constructed cell tracks for each gel type. The points are the sample means, $\bar{\xi}_i$, computed from Eq. A3. The solid lines represent the nonlinear regression fits of Eq. 36 to the data for the theoretical prediction $\langle d^2(t)\rangle$, providing direct estimates of the random motility coefficient, μ, and directional persistence time, P.

trend is observed, i.e. μ is not significantly affected by the presence of the supplements.

Another key assumption of the model is that cell penetration of the gel surface into the gel is a first-order process such that the probability per unit time of penetration is constant. Defining the surface residence time, τ, as the time spent on the surface before penetration, this assumption implies that the surface residence time distribution obeys an exponential distribution with parameter $\lambda = 1/k_+$:

$$F(t) = Prob(\tau \leq t) = 1 - \exp(-t/\lambda) \qquad (38)$$

The expected value of the residence time, $E(\tau)$, is then equal to $1/k_+$. A population of cells on the surface of each gel type was observed over a period of 24 h and the surface residence times for individual cells were recorded. An unbiased estimate for λ which includes cells which failed to penetrate the surface during the time of observation (type II censored data) is obtained from the ordered residence time data (i.e. $\tau_{(1)} < \tau_{(2)} < \ldots < \tau_{(m)}$) by the relation (16)

$$\lambda = \frac{1}{m}\left(\sum_{i=1}^{m} \tau_{(i)} + (n-m)\tau_{(m)}\right) \qquad (39)$$

where n is the total number of cells observed and m is the number of cells which penetrated the gel during the time of observation. The results of this analysis are presented in Table 1 (discussed below). As shown in Fig. 10 for each gel type, there is excellent agreement between the cumulative distribution of the experimental residence times and the theoretical cumulative distribution function, Eq. 38, using λ estimated from Eq. 39. This agreement supports the assumption that cell penetration of the collagen gel surface is indeed a first-order process.

Since $k_+ = 1/\lambda$, we also obtain *direct* estimates for the penetration rate constant for each gel type (presented in Table 1). These values are consistent with those estimated from the fits of the model solution to the experimental cell concentration profiles, i.e. as measured by k_+, type IV collagen significantly enhances cell invasion into the gel, whereas fibronectin inhibits cell invasion. As previously noted, the nonlinear regression performed to fit the model solution to the data presented in Fig. 2 indicates that cell invasion is "migration-limited" yielding a good estimate of the ratio $K = k_-/k_+$, but a poor estimate of k_+. Although the value of k_- is unknown, we can hypothesize that k_- depends primarily on cell behavior

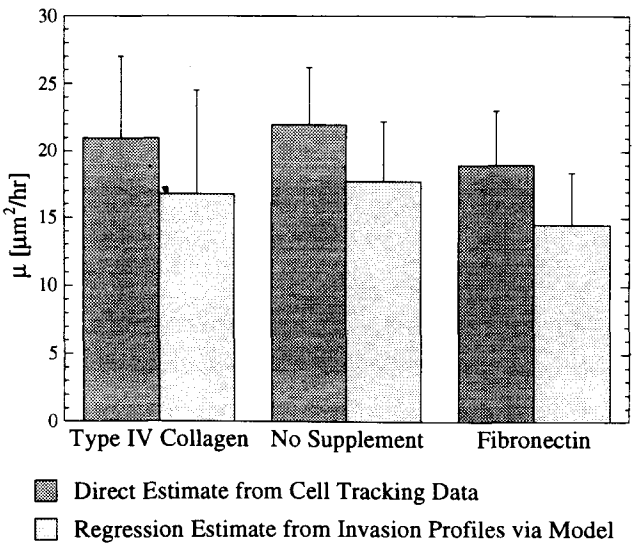

FIGURE 9. Comparison of values of μ estimated from the cell tracking analysis with those estimated by fitting the model solution to the experimental data presented in Fig. 2 for each gel type. Error bars represent standard errors in the estimates of μ from the regression analyses (Eqs. 9 and 10, Eq. 36).

TABLE 1. Surface residence time analysis for direct estimation of k_+.

Supplement	Counts n (mean)	k_+ (day^{-1})
Type IV collagen	75 (61)	1.77 ± 0.23*
No supplement	107 (79)	1.32 ± 0.15
Fibronectin	66 (41)	0.92 ± 0.14

*±Standard error of estimate.

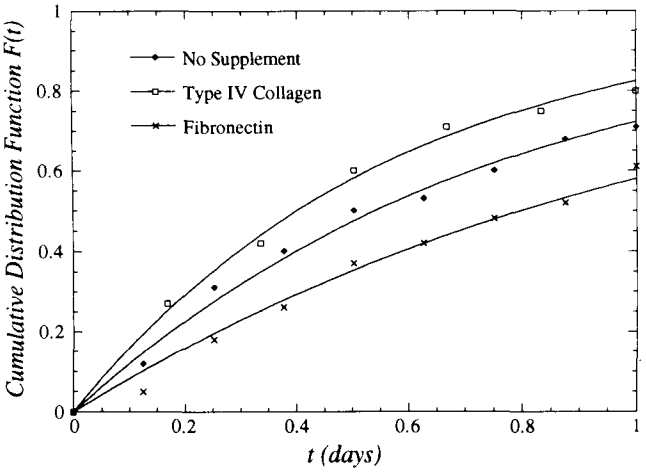

FIGURE 10. Comparison of measured cumulative distributions of surface residence time (points) for each gel type to the theoretical exponential distribution (lines) with parameter $\lambda = 1/k_+$.

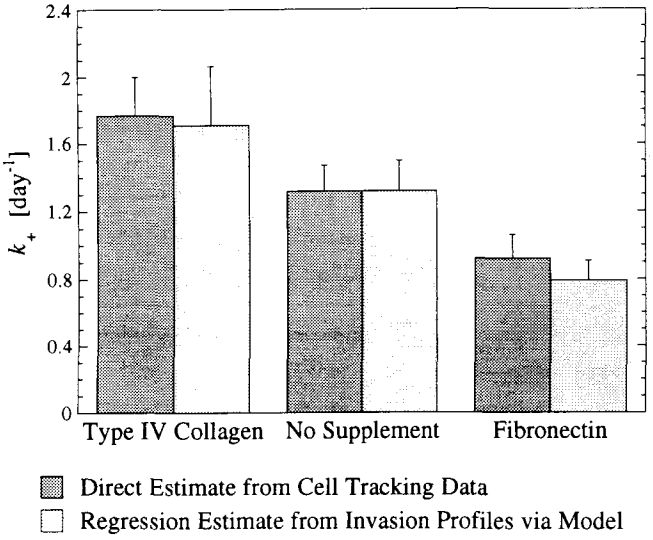

FIGURE 11. Comparison of values of k_+ estimated from the surface residence time analysis to those estimated by fitting the model solution to the experimental data presented in Fig. 2 for each gel type. The latter are calculated from the fitted values of K assuming that the values of k_- are the same for each gel type and equal to a value such that $k_+ = k_-/K$ equals the directly estimated value ($k_+ = 1/\lambda$) for the unsupplemented gel. Error bars represent standard errors in the estimates of k_+ from the regression analyses (Eqs. 9 and 10, Eq. 39).

within the gel. Considering our results for random migration within the gel (i.e. μ is independent of gel type), we hypothesize that the value of k_- is the same for each gel type and equal to a value such that $k_+ = k_-/K$ equals the directly estimated value $k_+ = 1/\lambda$ for the unsupplemented gel. This allows values for k_+ for the unsupplemented gels to be calculated from the regression estimates of μ and η (from the value of k_- so obtained and the regression estimate of K derived from μ and η in the "migration-limited" limit of Eq. 35) obtained by fitting the model solution to the experimental cell concentration profiles. Under this hypothesis, Fig. 11 shows that the directly estimated values of k_+ are in excellent agreement with those estimated via the model. This agreement again supports consistency of the model predictions of cell invasion with directly observed cell behavior; specifically, the type IV collagen supplement enhances cell penetration of the gel surface, whereas the fibronectin supplement inhibits penetration. Given the definition of our invasiveness index, η, the type IV collagen supplement is concluded to enhance invasiveness primarily by increasing k_+, and conversely for the fibronectin supplement.

Finally, we note that in the process of monitoring cell penetration of the gel surface in time-lapse for this analysis, we did observe frequent occurrences of cells returning to the surface (see Fig. A1b of the Appendix). Thus, although we did not estimate k_- directly, we can confirm that the associated event occurs, and given the self-consistency of our results, we conclude that it is approximated by a first-order process.

DISCUSSION

We present a mathematical model of the collagen gel invasion assay for systematic, objective interpretation of cell concentration profiles measured from cells invading the gel. The population of cells in the assay is modeled as a continuum, described by a concentration of cells on the gel surface, and a depth-dependent concentration of cells within the gel. Governing equations for the time evolution of these concentrations are formulated by assuming that, on the time scale of the assay, cell migration within the gel can be modeled as a diffusion process with a random motility coefficient, μ, cell penetration of the gel surface and return to the surface are first-order processes with interfacial transport rate constants k_+ and k_-, respectively, and cell division is a first-order process described by specific growth rate constants for the gel surface and interior, k_{gs} and k_g, respectively.

Assuming the values of k_{gs} and k_g are known, the solution to these equations is in terms of three phenomenological parameters: the penetration rate constant, k_+, which characterizes the efficiency with which cells penetrate the gel surface into the gel; the partition coefficient, $K = k_-/k_+$, which characterizes the equilibrium partitioning of cells on the gel surface relative to the gel interior (k_- characterizes the efficiency with which cells just below the gel surface return to the surface); and μ, which characterizes the efficiency of random migration of cells within the gel. In general, successful cell transport across the gel surface interface (i.e. invasion) requires cell penetration (measured by k_+) *and* migration away from the interface before returning to the surface (measured by the

ratio μ/K^2). Analysis of the general solution reveals that cell transport across the gel surface interface can be limited by either of these processes. We therefore define an index of invasiveness, η, in terms of these parameters, Eq. 34, that accounts for the sequence of cell penetration of *and* migration away from the gel surface interface for successful invasion, in analogy to resistances in series.

The model solution was fitted by nonlinear regression to the available cell concentration profiles for highly metastatic murine melanoma cells invading an unsupplemented type I collagen gel, a gel supplemented with type IV collagen, and a gel supplemented with fibronectin. In each case, the model yields excellent agreement with the data, and provides estimates for model parameters (Figs. 6 and 7). Comparison of estimates for η and μ for each gel type suggests that the supplements primarily modulate cell invasiveness (i.e. cell transport across the gel surface interface) rather than random migration within the gel.

We proceeded to independently validate key model assumptions and to directly estimate parameters for comparison to estimates obtained via the model. Time-lapse video microscopy of the gel surface and subsequent automated image analysis of the image sequences allowed measurement of the residence time of individual cells on the surface and construction of the two-dimensional projections of tracks of individual cells migrating within the gel. Analysis of the residence time distribution reveals that cell penetration does indeed conform to a first-order process (Fig. 10) and provides a *direct* estimate for k_+ for each gel type. These estimates agree closely with those determined from fitting the model solution to experimental cell concentration profiles, under the hypothesis that the value k_- is the same for each gel type (Fig. 11). Analysis of the tracks of cells within the gel supports the assumption that cell migration within the gel is random and can be modeled as a diffusion process (Fig. 8), and provides *direct* estimates for μ for each gel type that agree closely with values estimated via the model (Fig. 9).

Our evidence to support the validity of using k_+ and k_- in modeling cell penetration across the hypothesized gel surface interface is based on our observation that cells clearly settle onto a gel surface (i.e. all cells are in the same plane of focus) and that active penetration across the gel surface is accompanied by a clear change in focus (see Figs. A1 and A2). Indirect evidence is the success of the model in fitting the cell concentration profiles and the consistency between the model estimates and the direct estimates of k_+ under the reasonable hypothesis that k_- is the same for each gel type. While these do not constitute complete validation, electron microscope images such as those in (26) and (27), for example, provide evidence for an identifiable gel surface with respect to the cells, i.e. cells can be distinctly on top of or just beneath a layer of collagen fibrils. This further supports our view of distinct interfacial transport events for cells on top of and just beneath a gel surface interface as embodied in k_+ and k_-.

Although we focus on the collagen gel invasion assay, the model makes no assumptions about the composition of the model tissue. Therefore, we expect the model to apply equally well to any similar invasion assay where cells infiltrate a sufficiently thick, isotropic model tissue, for example, a fibrin gel (7,13,21). However, the mathematical solution we report here depends on the model assumption that a negligible number of cells are able to migrate completely through the model tissue over the duration of the assay. The model can easily be extended to address cell invasion assays in which transmigration through the model tissue is significant [such as for a reconstituted basement membrane (11)] by reformulation of the boundary condition for the bottom surface of the tissue. For example, if cells which exit the bottom of the tissue (of thickness L) do not re-enter the tissue, the boundary condition defined by Eq. 6 would be reformulated by matching the fluxes at the lower interface:

$$-\mu \frac{\partial c(L,t)}{\partial z} = k_- c(L,t) \tag{40}$$

The governing equations for the cell concentrations, $c(z,t)$ and $c_s(t)$, would need to be resolved accordingly.

There are limitations to the validity of this model. The primary one results from the assumption that cell invasiveness, migration, and growth are independent of cell concentration and constant throughout the duration of the assay. This implies that the effects of any accumulation of cell-derived stimuli are negligible and that the cells do not significantly alter the properties of the model tissue. In general, these limitations can be minimized by imposing judicious assay conditions such as a lower initial surface cell concentration and a shorter incubation period. The model assumptions are consistent with the possibility that cells on the gel surface are secreting proteolytic enzymes (10,31) or autocrine motility factors (17) which facilitate penetration of the gel surface, as long as the action of such mediators does not vary with incubation time. It is also possible that the underlying matrix itself significantly alters the cell behavior (2). However, if this alteration occurs on a time scale either much shorter or much longer than the time scale of the experiment, we expect this to have little effect on the validity of the model. The self-consistency of our model predictions with the available data suggests that these possible complications are not significant for the assay conditions employed.

Our results demonstrate that our model can be used to quantitatively and systematically interpret cell concentration profiles measured in the invasion assay via estimation of the model parameters. Since these parameters,

which characterize the underlying cell behavior, are objective, they can be legitimately used to compare results for different experimental conditions. Further, they enable a quantitative distinction between modulation of cell invasiveness (characterized by the invasiveness index, η) and modulation of cell migration within the gel (characterized by the random motility coefficient, μ) associated with altered gel composition by extracellular matrix supplements. This should prove to be a valuable tool in elucidating the regulation of cell invasion in metastasis and other physiological processes.

REFERENCES

1. Abramowitz, M.; Stegun, I.A., eds. Handbook of mathematical functions. Washington, D.C.: Department of Commerce; 1972.
2. Bissell, M.J.; Aggeler, J. Dynamic reciprocity: How do extracellular matrix and hormones direct gene expression? Prog. Clin. Biol. Res. 249:251–262; 1987.
3. Brown, A.F. Neutrophil granulocytes: Adhesion and locomotion on collagen substrata and in collagen matrices. J. Cell Sci. 58:455–467; 1982.
4. Crank, J. The mathematics of diffusion. Oxford: Clarendon Press; 1975.
5. Dickinson, R.B.; Tranquillo, R.T. Optimal estimation of cell migration indices from the statistical analysis of cell tracking data. AIChE J. 39(12):1995–2010; 1993.
6. Dunn, G.A. Characterizing a kinesis response: Time averaged measures of cell speed and directional persistence. Agents Act. Suppl. 12:14–33; 1983.
7. Erkell, L.J.; Schirrmacher, V. Quantitative in vitro assay for tumor cell invasion through extracellular matrix or into protein gels. Cancer Res. 48(23):6933–6937; 1988.
8. Faassen, A.E.; Schrager, J.A.; Klein, D.J.; Oegema, T.R.; Couchman, J.R.; McCarthy, J.B. A cell surface chondroitin sulfate proteoglycan, immunologically related to CD44, is involved in type I collagen-mediated melanoma cell motility and invasion. J. Cell Biol. 116(2):521–531; 1992.
9. Furukawa, M.; Kono, T.; Tanii, T.; Ishii, M.; Hamada, T.; Shibata, T. Proliferative potential of murine melanoma cells cultured in or on collagen gel. J. Dermatol. 17:297–302; 1990.
10. Goldfarb, R.H.; Liotta, L.A. Proteolytic enzymes in cancer invasion and metastasis. Semin. Thromb. Hemost. 12(4):294–307; 1986.
11. Hendrix, M.J.; Seftor, E.A.; Seftor, R.E.; Misiorowski, R.L.; Saba, P.Z.; Sundareshan, P.; Welch, D.R. Comparison of tumor cell invasion assays: human amnion versus reconstituted basement membrane barriers. Invas. Metast. 9(5):278–297; 1989.
12. Herbst, T.; McCarthy, J.B.; Tsilibary, E.C.; Furcht, L.T. Differential effects of laminin, intact type IV collagen, and specific domains of type IV collagen on endothelial cell adhesion and migration. J. Cell Biol. 106:1365–1373; 1988.
13. Islam, L.N.; McKay, I.C.; Wilkinson, P.C. The use of collagen or fibrin gels for the assay of human neutrophil chemotaxis. J. Immunol. Methods 85(1):137–151; 1985.
14. Kleinman, H.K.; McGarvey, M.L.; Liotta, L.A.; Geron Robey, P.; Trygvasson, K.; Martin, G.R. Isolation and characterization of type IV procollagen, laminin, and heparan sulfate proteoglycan from the EHS sarcoma. Biochem. 21:6188–6193; 1982.
15. Lackie, J.M.; Chaabane, N.; Crocket, K.V. A critique of the methods used to assess leucocyte behaviour. Biomed. Pharmacother. 41(6):265–278; 1987.
16. Lawless, J.F. Statistical models and methods for lifetime data. New York: Wiley; 1982.
17. Liotta, L.; Schiffmann, E. Tumor autocrine motility factors. Important Adv. Oncol. 17–30; 1988.
18. Liotta, L.; Rao, C.N.; Barsky, S.H. Tumor invasion and the extracellular matrix. Lab Invest. 49(6):636–649; 1983.
19. McCarthy, J.B.; Chelberg, M.K.; Mickelson, D.J.; Furcht, L.T. Localization and chemical synthesis of fibronectin peptides with melanoma adhesion and heparin binding activities. Biochemistry 27(4):1380–1388; 1988.
20. McCarthy, J.B.; Sas, D.F.; Furcht, L.T. Mechanisms of parenchymal cell migration into wounds. In: Clark, R.A.F., Henson, P.M., eds. The molecular and cellular biology of wound repair. New York: Plenum Press; 1988. pp. 281–308.
21. Montesano, R.; Pepper, M.S.; Vassalli, J.D.; Orci, L. Phorbol ester induces cultured endothelial cells to invade a fibrin matrix in the presence of fibrinolytic inhibitors. J. Cell Physiol. 132(3):509–516; 1987.
22. Mooradian, D.L.; McCarthy, J.B.; Komanduri, K.V.; Furcht, L.T. Effects of transforming growth factor-beta 1 on human pulmonary adenocarcinoma cell adhesion, motility, and invasion in vitro. J. Natl. Cancer Inst. 84(7):523–527; 1992.
23. Othmer, H.G.; Dunbar, S.R.; Alt, W. Models of dispersal in biological systems. J. Math. Biol. 26(3):263–298; 1988.
24. Runyan, R.B.; Markwald, R.R. Invasion of mesenchyme into three-dimensional collagen gels: A regional and temporal analysis of interaction in embryonic heart tissue. Dev. Biol. 95(1):108–114; 1983.
25. Russo, R.G.; Thorgeirsson, U.; Liotta, L.A. In vitro quantitative assay of invasion using human amnion. In: Liotta, L.A., Hart, I.R., eds. Tumor invasion and metastasis. Boston: Nijhoff; 1982. pp. 175–187.
26. Schor, S.L.; Allen, T.D.; Harrison, C.J. Cell migration through three-dimensional gels of native collagen fibres: Collagenolytic activity is not required for the migration of two permanent cell lines. J. Cell Sci. 41:159–175; 1980.
27. Schor, S.L.; Allen, T.D.; Winn, B. Lymphocyte migration into three-dimensional collagen matrices: A quantitative study. J. Cell Biol. 96(4):1089–1096; 1983.
28. Schor, S.L.; Schor, A.M.; Winn, B.; Rushton, G. The use of three-dimensional collagen gels for the study of tumour cell invasion in vitro: Experimental parameters influencing cell migration into the gel matrix. Int. J. Cancer. 29(1):57–62; 1982.
29. Seber, G.A.F.; Wild, C.J. Nonlinear regression. New York: John Wiley & Sons; 1989.
30. Smith, C.W.; Anderson, D.C. PMN adhesion and extravasation as a paradigm for tumor cell dissemination. Cancer Metast. Rev. 10(1):61–78; 1991.
31. Trygvasson, K.; Hoyhtya, M.; Salo, T. Proteolytic degradation of extracellular matrix in tumor invasion. Biochim. Biophys. Acta. 907(3):191–217; 1987.

NOMENCLATURE

$c(z,t)$	= cell concentration within the gel
c_s	= cell concentration on the gel surface
$\langle d^2(t) \rangle$	= theoretical mean-squared cell displacement (36)

J = cell flux (2)
k_+ = rate constant for cell penetration of the gel surface (entering the gel)
k_- = rate constant for cell penetration of the gel surface (returning to the gel surface)
k_g = rate constant for cell division of cells within the gel
k_{gs} = rate constant for cell division of cells on the gel surface
$K = k_-/k_+$ = equilibrium partition coefficient for cells on the gel surface to cells within the gel
n_j = number of time steps which cell j was tracked
N = total number of cell tracks
N_i = measured number of cells/cm^2 in a 20 μm increment of gel depth from z_{i-1} to z_i
N_{ti} = total number of averaged track segments comprised of i time increments
$N(t_k)$ = number of presently tracked cells at time point t_k
P = directional persistence time of cell movement
s_i^2 = sample variance of squared displacement based on track segments comprised of i time increments (A5)
t = time
$\underline{x}$ = position of presently tracked cell
$\underline{y}$ = position of unmatched cell
$\mathbf{x}(t_k) = [\underline{x}_1 \ldots \underline{x}_N]$ = the array of cell positions of presently tracked cells at time point t_k
$\mathbf{y}(t_{k+1}) = [\underline{y}_1 \ldots \underline{y}_M]$ = the array of (unmatched) cell positions at time point t_{k+1}
z = depth into the gel
δ = self-similar variable (12)
ϵ_i = residual between sample mean and theoretical mean squared displacement at time t_i
ϕ^2 = ratio of the time scale of cell transport away from the gel surface interface via migration (K^2/μ) to the time scale of cell penetration of the surface ($1/k_+$) (15)
η = invasiveness index (34)
λ = parameter of the exponential distribution (38)
μ = cell random motility coefficient (2,36)
$\bar{\xi}_i$ = sample mean of the squared displacement based on track segments comprised of i time increments (A3)
σ_i^2 = variance of ϵ_i (A6)
$\tau_{(i)}$ = surface residence time of i^{th} cell observed to penetrate the gel surface

APPENDIX – MATERIALS AND METHODS

Cell Culture

The cell line used in these studies was the highly metastatic clone M4 of the K-1735 amelanotic melanoma. Cells were grown and passaged from frozen stocks in DMEM containing 10% calf serum as described previously (19), and the number of *in vitro* passages was limited to 10 in order to minimize phenotypic drift.

Preparation of Type IV Collagen and Fibronectin

Type IV collagen was purified from EHS tumor grown in lathyritized mice as described previously (12) based on the protocol of Kleinman et al. (14). Fibronectin was purified from a by-product of factor VIII production by sequential ion exchange and gelatin affinity chromatography as described previously (19). Both proteins were greater than 95% pure based on staining by Coomasie Blue.

Collagen Gel Invasion Assays Used in Obtaining Data Presented in Fig. 2

Native type I collagen gels were prepared under sterile conditions using a protocol described previously (8), modified from that of Schor et al. (26). Gels were reconstituted from Vitrogen 100 (Celtrix Laboratories, Santa Clara, CA) at a final concentration of 2.2 mg/ml. Supplement proteins in phosphate buffered saline were added in 1 ml volumes to this mixture, yielding final concentrations of 20 μg/ml for fibronectin and 75 μg/ml for type IV collagen (these concentrations exhibited maximal modulation of cell concentration profiles). The physical nature of the inclusion of the protein supplements in the type I collagen gel was not investigated, but it was determined that the mean diameter of the type I collagen fibrils was not significantly affected (McCarthy, unpublished data). Reported cell number, N_i, at any depth level z_i in Fig. 2 is the number of cells/cm^2 in a 20 μm increment of depth Δz from z_{i-1} to z_i.

Estimation of Specific Growth Rate Constants

Specific growth rate constants were estimated from cell doubling time on type I collagen films with or without

protein supplements in the same conditions used in the invasion assays. The specific growth rate was unaffected by presence of supplements, with $k_{gs} = 0.23$ day^{-1} in each case. Specific growth rates were assumed to be the same within the gel as on the gel surface, that is $k_g = k_{gs}$. This assumption is consistent with existing data for murine melanoma cells (9).

Nonlinear Regression Fit of Model Solution to Experimental Cell Concentration Profiles

The cell concentration profile, $c(z,t)$, was estimated from the experimental cell concentration profile (Fig. 2) by the trapezoidal approximation, $c_i = c((z_i - 0.5\Delta z, t) = N_i/\Delta z$. Surface cell density, $c_s(t)$, was not measured and therefore was estimated from a cell balance by subtracting the total number of cells/cm^2 within the gel from the expected total number of cells/cm^2 on the surface and interior of gel, based on the estimated specific growth rate, k_g, i.e.

$$c_s(t) = e^{k_g t} c_{s0} - \sum_{i=1}^{\infty} N_i(t) \qquad \text{(A1)}$$

A nonlinear least squares regression fit of the model solution to the data was performed to obtain estimates for the three unknown model parameters (k_+, K, and μ). Errors in the parameter estimates were estimated from the asymptotic variance-covariance matrix obtained from the nonlinear regression analysis (29).

Time-Lapse Video Microscopy and Cell Tracking

For direct observation of cell behavior, the surface of the collagen gel was monitored using time-lapse video microscopy. A Zeiss Axiovert 10 inverted optical microscope (10× objective and 2.5× Optovar lens) with motorized stage and focus for automated x, y, and z positioning control (Carl Zeiss, Inc., Thornwood, NY) was used. Bright field optics allowed observation of cells both on the gel surface (in-focus) and within the gel (out-of-focus, but quite visible). Images were obtained with a Hamamatsu C2400 Newvicon video camera (Hamamatsu, Bridgewater, NJ) and stored with an on-line Panasonic TQ-2028-F optical disc recorder (Panasonic, Secaucas, NJ). Automated image acquisition and stage movement were directed via commands from a Kontron IBAS image analysis system (Kontron Elektronik, Eching, Germany). A program was written in the IBAS interpreter language to simultaneously monitor multiple fields in time-lapse and store the resultant images in the proper sequence on optical disc. Images at 15 min intervals were obtained in five randomly selected fields for each gel type. To allow for atmospheric CO_2 conditions, DMEM was buffered with 20 mM HEPES instead of sodium bicarbonate. Gels were kept at 37 ±

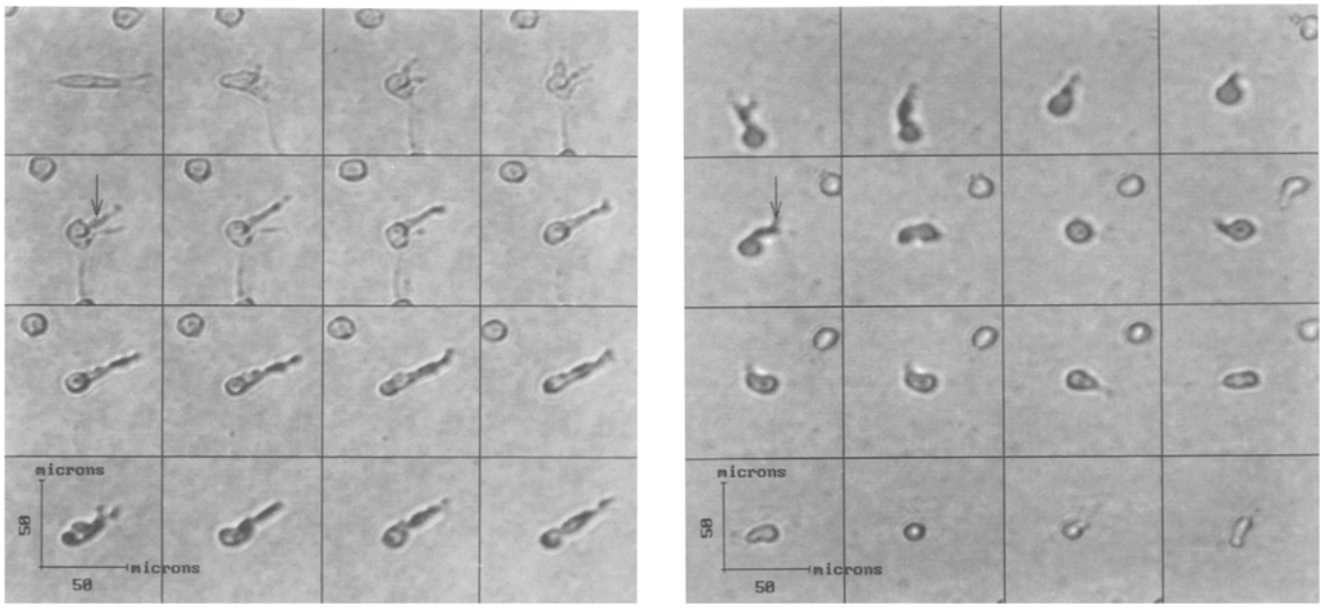

(a) (b)

FIGURE A1. Sequence of time-lapse video images showing examples of (a) cell penetration of the gel surface into the gel and (b) return to the surface. Cells on the surface are distinguished as in-focus. The arrows indicate extension of cell pseudopodia. A 10-min time-lapse interval was used. In (a), the pseudopod extends beneath the gel surface and aids in pulling the cell into the gel. The video images are zoomed from the low magnification images acquired for direct estimation of k_+ and μ, and consequently are not of optimal resolution.

1°C with an air stream incubator as monitored by a sterile temperature probe inserted into one well of the tissue culture chamber.

Sequences of images for each gel type were replayed to measure the surface residence time of individual cells selected at random. They were followed by manual observation until they penetrated the gel surface. This event was easily observable as a cell would first extend pseudopodia beneath the surface, then move out of the focal plane of the gel surface becoming distinctly out-of-focus (Fig. A1a). The time at penetration was recorded as the surface residence time.

To track cells within the gel, another program was written in the IBAS interpreter language to measure and store the centroid of the projected cell area of cells within the gel at each frame of the recorded sequence. Projected cell areas were measured from a binary image obtained by several standard image processing steps, as shown in Fig. A2. First the original gray level image was processed with a highpass filter to remove any low frequency shading differentials. The resulting gray level image was made binary by using a threshold to discriminate the darker cells from the lighter background of the gel. Any "holes" in the binary images of the cells were then filled. Any touch-

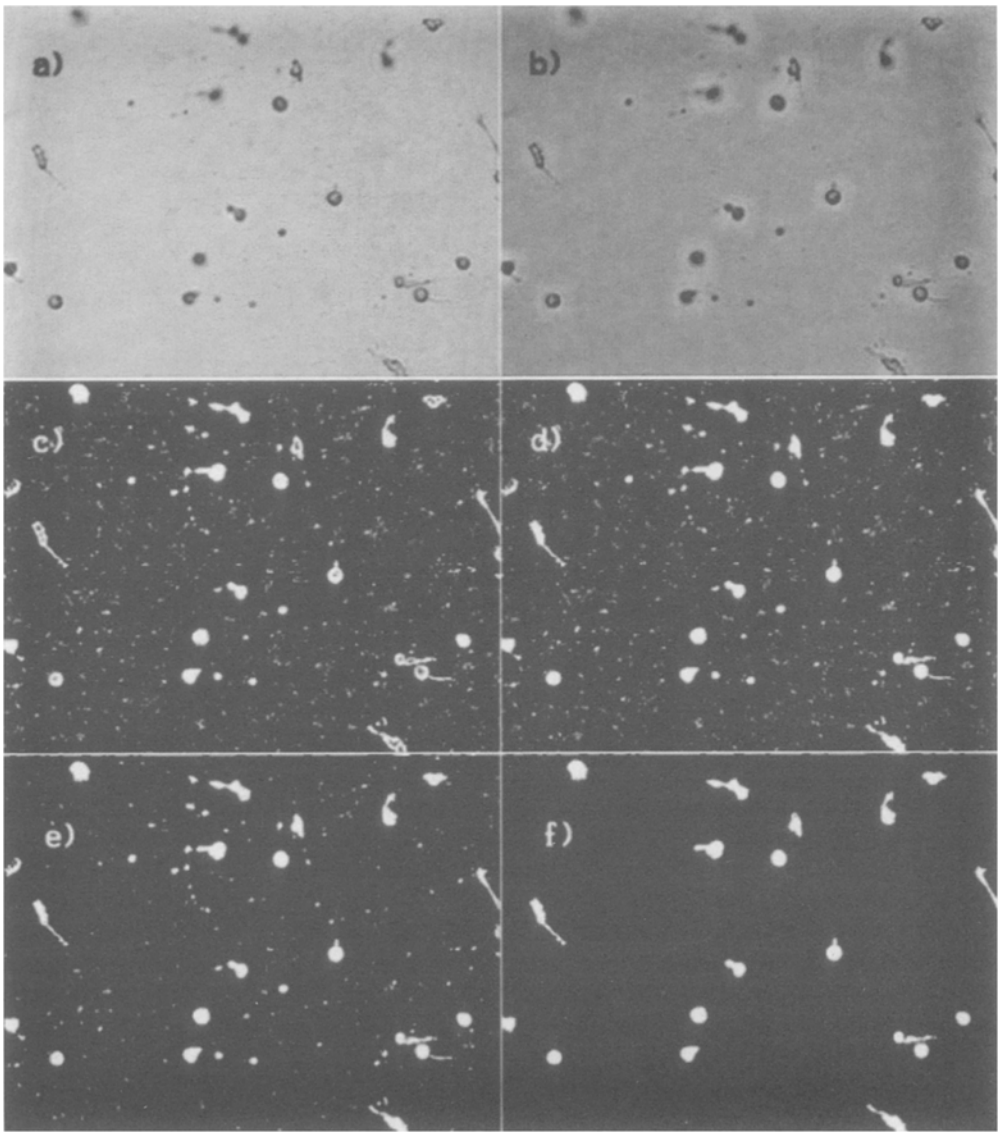

FIGURE A2. Sequence of images demonstrating the required sequence of image processing steps in the development of a binary image from an original gray level image. (a) The original gray level image. (b) Large-band highpass-filtered image with low frequency shading removed. (c) Resultant binary image. (d) Binary image with holes in objects filled. (e) Binary image in (d) after erosion and dilation. (f) Binary image in (e) after removing background noise (small objects). See text for details.

ing cells were then separated with erosion and dilation of the binary objects in the image. Finally, any remaining binary objects which did not correspond to an area of reasonable value for a cell ($30\ \mu m^2 < \text{Area} < 500\ \mu m^2$) were removed, and the centroid locations of the remaining objects (presumably cells) were then measured.

Cells within the gel were distinguishable from cells on the gel surface by the degree to which cells were in-focus. "In-focus information" was quantified with the following algorithm (Fig. A3): low spatial frequency information ("blur") was removed from the original image with a highpass filter and the resulting image was then made binary. Few pixels remained in this binary image within the corresponding projected areas of out-of-focus cells, and many pixels remained for cells in-focus. Therefore, cells on the surface could be discriminated from those within the gel based the ratio of the resultant number of in-focus pixels to the number of pixels in the original projected cell area. The threshold ratio in this discrimination was calibrated empirically by comparison to original images.

The array of centroid positions of cells within the gel at each time point was stored in a database and transferred to an Apollo workstation. A FORTRAN program was written to construct cell tracks from this time series data using an algorithm which attempts to match the elements of the arrays of cell positions between time points (Fig. A4). Let $\mathbf{x}(t_k) = [\underline{x}_1 \ldots \underline{x}_N]$ be the array of cell positions, $\underline{x}_j$, $j = 1$ to $N(t_k)$, of $N(t_k)$ presently tracked cells at time point t_k. Let $\mathbf{y}(t_{k+1}) = [\underline{y}_1 \ldots \underline{y}_M]$ be the array of new cell positions at the next time point, t_{k+1}. We attempt to continue the current cell tracks by "matching" $\mathbf{y}(t_{k+1})$ to $\mathbf{x}(t_k)$ to obtain $\mathbf{x}(t_{k+1})$. This is accomplished by finding the two elements of $\mathbf{y}(t_{k+1})$ and $\mathbf{x}(t_k)$ which are nearest, i.e., those which minimize $\|\underline{y}_m - \underline{x}_j\|$, j = 1 to $N(t_k)$, $m = 1, M$. These elements are then matched and removed from eligibility for further matching. This process is repeated until all elements from either ar-

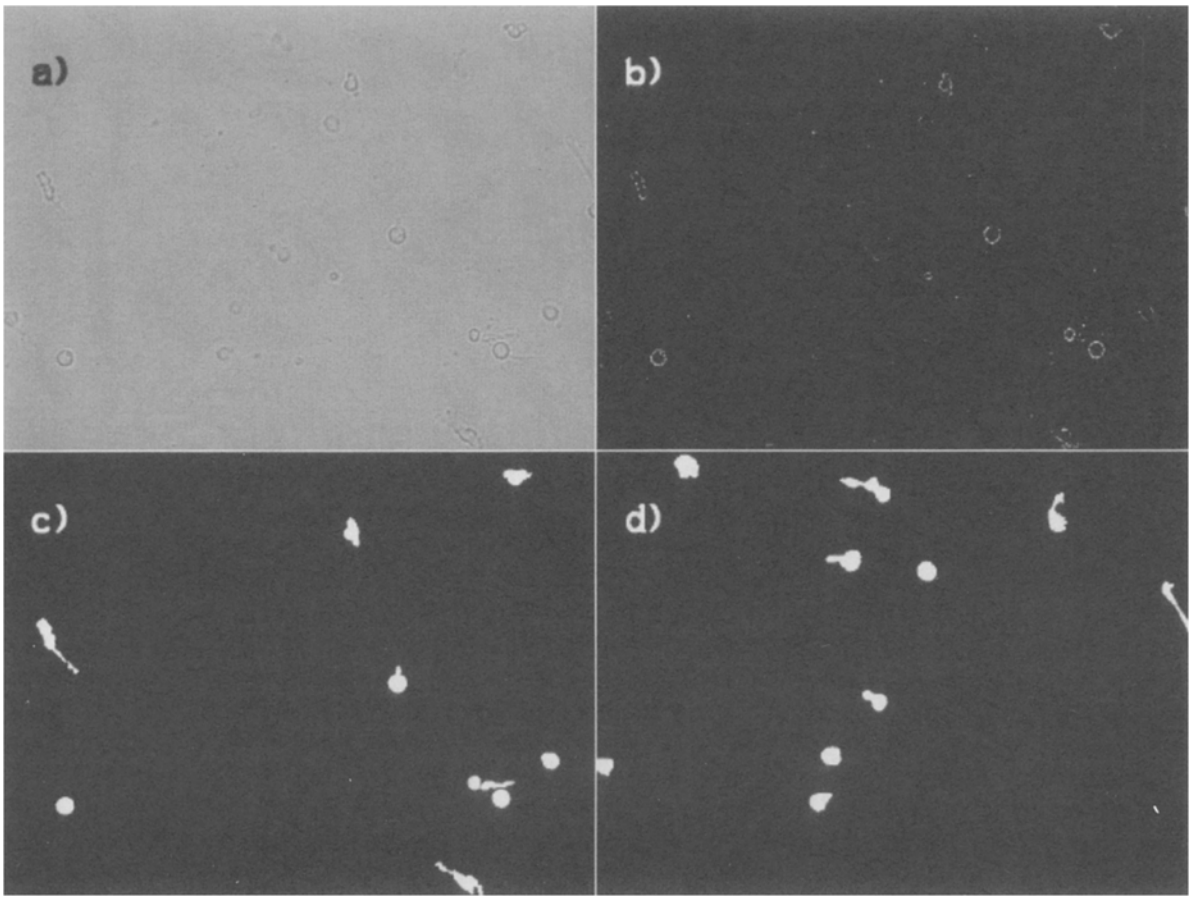

FIGURE A3. Sequence of images demonstrating the required sequence of image processing steps in quantifying the amount of "in-focus information" of individual cells. The original gray level image is the same as in Fig. A2a. (a) Small-band highpass-filtered image, retaining only in-focus details. (b) Resultant binary image. (c) Objects for Fig. A2f deemed in-focus, after comparison to binary image (b). (d) Objects of Fig. A2f deemed out-of-focus, after comparison to binary image (b). See text for details.

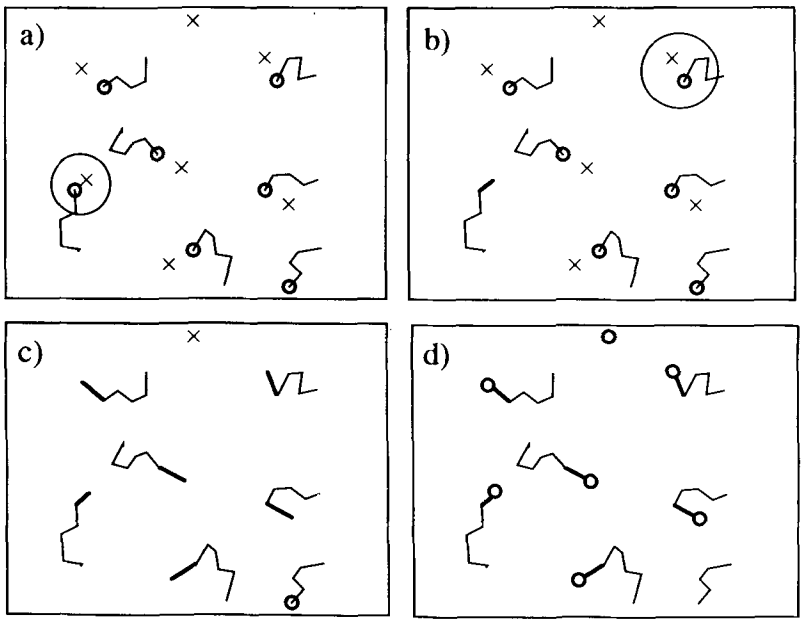

FIGURE A4. Steps in the matching algorithm to simultaneously track multiple cells from a hypothetical sequence of images. (a) Cell positions at time t_i, $\mathbf{x}(t_i)$, are represented by ○, and those at t_{i+1}, $\mathbf{y}(t_{i+1})$, by ×. The constructed track associated with each ○ is indicated by the thin connected segments. The distances between each unmatched ○ and all ×'s are computed and compared to determine the nearest ×-neighbor. When an ○ and × are matched (see large circle showing successful match) they become ineligible for further matching. (b) The continuation of the track associated with the match shown in (a) is indicated by the connecting thick segment. Another successful match is shown. (c) This matching and track continuation process is repeated until all ○'s are matched, or until all nearest-neighbor distances exceed some maximum allowable distance. In this example, one unmatched element of both $\mathbf{x}(t_i)$ and $\mathbf{y}(t_{i+1})$ remain. (d) The tracks corresponding to all unmatched ○'s are terminated, and the cell positions corresponding to all unmatched ×'s are used to begin new tracks (one instance of each case in this example). See text for further details.

ray have been matched, or until a maximum distance, $\|\underline{y}_m - \underline{x}_j\|_{\max}$, is exceeded (based on the $\Delta t = 15$ min time-lapse increment and the maximum possible cell speed, taken to be 3 μm/min in this case). If $N > M$, cells corresponding to unmatched elements of $\mathbf{x}(t_k)$ are considered "lost" at time point t_k, and are ineligible for future matching, and the cell track to that point, $[\underline{x}_j(t_0) \ldots \underline{x}_j(t_k)]$, is then terminated and stored in a database for later analysis. If $M > N$, unmatched elements of $\mathbf{y}(t_{k+1})$ are used as the beginnings of new cell tracks. The final result of this procedure is a set of cell tracks corresponding to various lengths of time. This procedure was applied to the five monitored fields of each gel type, containing between 10 and 30 cells per field.

The robustness of this matching algorithm depends on several factors, including the cell density in the image, the time-lapse increment, the cell movement properties, and the effectiveness of the sequence of image processing steps in discriminating individual cells. A measure of the robustness is the average of the constructed track length, $\langle T \rangle$ (number of time increments), which is inversely proportional to the number of cells lost per time increment in the matching process. For these studies, $\langle T \rangle$ ranged from 15 to 25 time-increments (3.75-6.25 h), depending on the field. Actual (vs. constructed) cell tracks with large displacements are more likely to be lost in the matching process; therefore, we minimized any bias resulting from preferential weighting of cell tracks with small displacements, which are less likely to be lost in the matching process, by only considering time intervals less that $\langle T \rangle$ in the following analysis.

Constructed tracks were subsequently analyzed to obtain mean-squared displacement data. To do so, we estimated the statistics of the random variable, ξ_i, the squared displacement over i time increments of a cell track. Let $\xi_{ik}^{(j)}$ be a sample of ξ_i, i.e. the squared displacement from t_k to t_{i+k} for cell track j:

$$\xi_{ik}^{(j)} = \|\underline{x}_j(t_{k+i}) - \underline{x}_j(t_k)\|^2 \tag{A2}$$

Then $\bar{\xi}_i$, the sample mean of ξ_i, was obtained by averaging over non-overlapping time intervals of the cell tracks using

$$\bar{\xi}_i = \frac{1}{N_{ti}} \sum_{j=1}^{N} \sum_{k=0;\,step\ i}^{n_j - i} \xi_{ik}^{(j)} \tag{A3}$$

where N is then total number of cell tracks, n_j is the number of time increments that comprise cell track j, and

N_{ti} is the total number of averaged track segments comprised of i time increments, given by

$$N_{ti} = \sum_{j=1}^{N} \left[\frac{n_j - i}{i} \right] \tag{A4}$$

The square brackets signify the maximum integer less than or equal to the value therein. Since non-overlapping intervals were used, the sample variance of the squared displacement, s_i^2, is

$$s_i^2 = \frac{1}{N_{ti} - 1} \sum_{j=1}^{N} \sum_{k=0;step\ i}^{n_{j-1}} (\xi_{ik}^{(j)} - \bar{\xi}_i)^2 \tag{A5}$$

Since more segments of the cell tracks are available for averaging for the smaller time increments, t_i, the residuals in the regression, $\epsilon_i = \bar{\xi}_i - \langle d^2(t_i) \rangle$ are not identically distributed random variables, but instead have probability distributions that depend on t_i, as well as the number and lengths of the cells tracks used in the averaging process. To provide statistically optimal estimates of P and μ, a generalized least squares fit of Eq. 36 to the $(\bar{\xi}_i, t_i)$ data is necessary (29), which weights the residuals according to their variance, $\sigma_i^2 = \langle \epsilon_i^2 \rangle$, where

$$\sigma_i^2 = \frac{s_i^2}{N_{ti}} \tag{A6}$$

To obtain regression estimates for μ and P, the residuals, ϵ_i were weighted by $1/\sigma_i$. A more general weighting scheme which accounts for inherent correlation between the ϵ_i is possible (5); however, for the large number of statistically independent cell tracks averaged, this more complex scheme was deemed unnecessary.

AUTHOR PROFILES

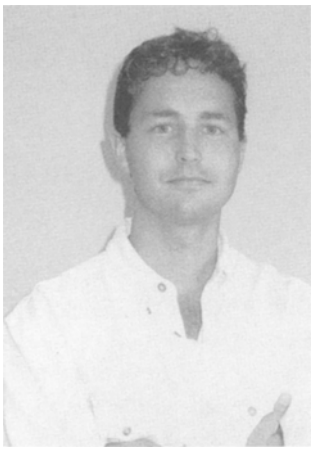

Richard B. Dickinson, Ph.D., earned his doctorate in chemical engineering from the University of Minnesota in 1992 and was a postdoctoral research associate for one year in the Department of Chemical Engineering at the University of Wisconsin. He is currently a NATO Postdoctoral Fellow in the Department of Theoretical Biology at the University of Bonn, and becomes an Assistant Professor in the Department of Chemical Engineering at the University of Florida in the Fall of 1994, working on problems associated with cell adhesion, cell motility, and cell-biomaterial interactions.

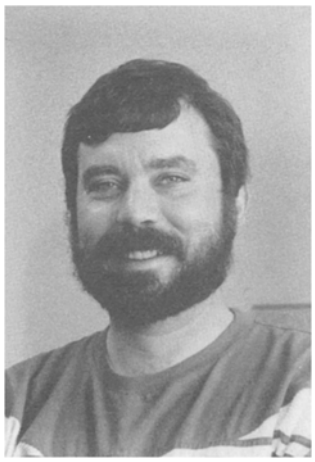

James B. McCarthy, Ph.D., received his B.A. from Susquehanna University, Selinsgrove, PA, in 1974 and his Ph.D. in 1981 from Catholic University of America, Washington, D.C. He was a Postdoctoral Fellow in the laboratory of Dr. Leo Furcht at the University of Minnesota from 1981 to 1983. He began as an Assistant Professor in the Department of Laboratory Medicine & Pathology at the University of Minnesota in 1984. Dr. McCarthy is currently an Associate Professor in Laboratory Medicine & Pathology and the Biomedical Engineering Center studying the structure and function of the extracellular matrix in tumor cell motility and invasion.

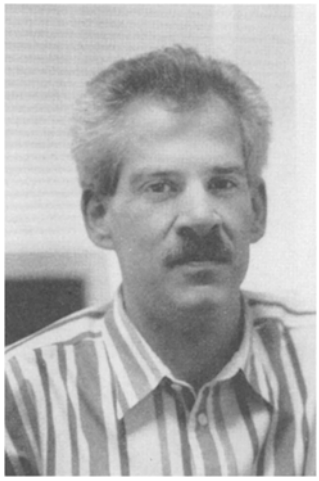

Robert T. Tranquillo, Ph.D., received his doctorate in chemical engineering from the University of Pennsylvania in 1986 and was a NATO Postdoctoral Fellow for one year at the Centre for Mathematical Biology at Oxford University. He began his position as Assistant Professor in the Department of Chemical Engineering & Materials Science at the University of Minnesota in 1987, being promoted to Associate Professor in 1993. His research focuses on quantitative approaches to problems in cellular and tissue engineering.